batteries

MDPI

Article

Revealing Relationship Between In Situ Impedance and Lithium Plating Onset Based on Lithium–Graphite Half-Cells

Zhao Jiang [1,2], Jiangwei Wang [3], Haiwei Li [2], Bingyin Luo [4], Wentao Wu [3], Xueyuan Wang [3,*], Haifeng Dai [3], Jianjun Jiang [1,*] and Xuezhe Wei [3]

1 School of Mechanical Engineering, Northwestern Polytechnical University, Xi'an 710072, China; cj@joyson.cn
2 Ningbo Joyson Advanced Energy Research Institute Co., Ltd., Ningbo 315040, China; hw.li@joyson.cn
3 School of Automotive Studies, Tongji University, Shanghai 201804, China; 2332902@tongji.edu.cn (J.W.); 2133543@tongji.edu.cn (W.W.); tongjidai@tongji.edu.cn (H.D.); weixzh@tongji.edu.cn (X.W.)
4 Integrated Circuit R&D Center, ICBG China Resources Microelectronics Co., Ltd., Shanghai 200072, China; luoby@powtech.crmicro.com
* Correspondence: 7wangxueyuan@tongji.edu.cn (X.W.); jianjun@nwpu.edu.cn (J.J.)

Abstract: Lithium plating may occur during charging, especially at high rates or overcharging conditions for lithium-ion batteries (LIBs), which would cause battery capacity degradation and even trigger thermal runaway. Thus, it is essential to detect lithium plating onset during the charging processes. Electrochemical impedance can reveal the dynamic electrode properties of the battery, which is promising for use in battery management systems for the online detection of lithium plating onset. In this article, the impedance at 1 Hz is measured during the over-discharge and fast discharge processes using lithium–graphite half-cells. For half-cells, the variation in graphite electrode potential vs. Li/Li^+ during discharging is directly recorded. An equivalent circuit model is proposed and adopted to estimate the real lithium plating reaction overpotential, which is deemed the thermodynamic indicator of lithium plating and is used as validation for the detection of lithium plating onset. Through the auxiliary validation of the estimation of lithium plating overpotential and the shape of incremental capacity curves, the relationship between impedance changes at specific frequency and the lithium plating onset is revealed. The results lay a good foundation for proposing the online diagnostic method of lithium plating onset based on the in situ impedance.

Keywords: lithium-ion batteries; impedance; lithium plating; diagnosis

check for updates

Citation: Jiang, Z.; Wang, J.; Li, H.; Luo, B.; Wu, W.; Wang, X.; Dai, H.; Jiang, J.; Wei, X. Revealing Relationship Between In Situ Impedance and Lithium Plating Onset Based on Lithium–Graphite Half-Cells. *Batteries* **2024**, *10*, 410. https://doi.org/10.3390/batteries10120410

Academic Editor: Wojciech Mrozik

Received: 29 September 2024
Revised: 12 November 2024
Accepted: 21 November 2024
Published: 23 November 2024

Copyright: © 2024 by the authors. Licensee MDPI, Basel, Switzerland. This article is an open access article distributed under the terms and conditions of the Creative Commons Attribution (CC BY) license (https://creativecommons.org/licenses/by/4.0/).

1. Introduction

Lithium-ion batteries (LIBs) have been widely used in recent years, especially in the field of electric vehicles [1]. In order to solve users' range anxiety, fast charging technology for lithium-ion batteries has been emphasized. However, high-rate charging and overcharging are major reasons for the lithium plating of LIBs [2,3]. Due to the rate limitations of the solid or liquid phase mass transfer speed, lithium plating occurs when the overpotential of the lithium plating reaction on the graphite electrode drops below 0 V (vs. Li/Li^+) [4,5]. The plated lithium may further react with the electrolyte, leading to a decrease in the amount of cyclable lithium [6–8]. Moreover, the plated lithium metal will possibly gradually grow through the separator, which could cause internal short circuits and even trigger thermal runaway [9,10]. Thus, it is essential to detect the onset of lithium plating timely during the charge process.

The detection methods for lithium plating can be divided into ex situ methods and in situ methods. Most ex situ methods require disassembling the battery. For example, optical microscopy [11,12] and electron microscopy [13] can be used to check the surface of the anode of the battery to determine if lithium plating has occurred. Nuclear magnetic resonance (NMR) has also been utilized for lithium plating detection [14,15]. However, these methods mentioned above are mostly not suitable for the online detection of lithium

plating and can also not determine the exact time point during charging process at which lithium plating occurs.

Typically, in situ methods for lithium plating detection are easier to operate and more applicable for real-time charging process control. Regularly used techniques include the battery models [16], differential voltage analysis [17,18], incremental capacity (IC) analysis [19], electrochemical impedance [20,21], deep learning methods [22], and so on. Arora et al. [16] integrated the lithium plating reaction into the classical pseudo-two-dimensional (P2D) battery model [23], which requires heavy computation. Lu et al. [24] established equivalent circuit models for the cathode and anode, respectively, to estimate the potential of the battery anode (vs. Li/Li^+) and use it to control the charge process. Zhao et al. [25] also built equivalent circuit models for each electrode and improved the estimation accuracy of anode potential by switching different circuit models at different charging stages. Wang et al. [22] utilized deep learning techniques to predict the anode potential in real time, with battery terminal voltage, current, and temperature as input. The re-intercalation process of plated lithium can form a plateau in the voltage curve, so differential analysis of the voltage can also effectively detect lithium plating [26–28]. For example, Smart et al. [29] analyzed the plateau and believed that there is a distinct relationship between the length of the plateau and the amount of lithium plating. Chen et al. [30] proposed a combined strategy based on the complementarity of variance entropy and voltage plateau, successfully identifying the abnormal lithium plating cell from a series-connected battery pack.

The impedance method is non-destructive and can be easily implemented with only current and voltage response signals. Harting et al. [31] observed the correlation between the increase in the third harmonic voltage response of the battery and lithium plating through nonlinear frequency response analysis (NFRA) under high-rate current input. Chen et al. [32] found that lithium plating leads to a decrease in the peak intensity of the anode charge transfer reaction in the distribution of relaxation times (DRT) curve, which might be used as an indicator for lithium plating. Brown et al. [33] also used the DRT to detect the onset of lithium plating during the fast charging process and believed that the increase in the solid–electrolyte interface (SEI) resistance is an indicator of lithium plating. Wang et al. [34] utilized the difference between the relaxation voltage curve fitted by the DRT model and the actual voltage curve to identify the cell with lithium plating. The accuracy is high, but the exact time point for lithium plating during charging cannot be determined. Sun et al. [35] introduced a 10 s rest every 5% state of charge (SOC) during the charging to acquire the internal impedance of the cell and found the normalized impedance of cells with lithium plating shows abnormal decrease at the late charging process, and differential voltage curves of the relaxation period after charging were used as cross-validation. However, the 10 s rest slows down the whole charging process. Koseoglou et al. [36] superimposed sinusoidal current on the charging current to acquire dynamic impedance within wide frequency ranges and extracted several characteristic impedances to detect lithium plating. They found that when lithium plating occurs, these characteristic impedances show abnormal change trends. Differential voltage curves were also analyzed as supplementary validation. Our previous work [37] reached conclusions that are similar to the previously mentioned papers and found the impedance at a specific frequency abnormally decreases during charging when lithium plating occurs. The differential voltage method was also used as auxiliary verification. Shen et al. [38] combined the abnormal impedance change with long short-term memory networks to reduce the time delay in online lithium plating detection.

While the articles [35–38] mentioned above use the differential voltage curve of the relaxation period after the charging to indicate that abnormal trends in the impedance curve during charging signify the occurrence of lithium plating, the differential voltage is recorded only after the entire charging process. Therefore, using the differential relaxation voltage method cannot sufficiently prove that the abnormal change point in the impedance curve is exactly the onset time point of lithium plating. Article [21] discussed the abnormal impedance decrease and used the abnormal drop in dV/dQ curve and the obvious

increased swelling force to confirm the lithium plating time point. Lithium plating overpotential is believed to be the thermodynamic indicator of whether lithium plating can occur. To directly verify the relationship between lithium plating onset and abnormal impedance changes, the lithium–graphite half-cells (coin cell format) are used in this paper so that the anode potential can be directly measured. However, the measured anode potential is not equivalent to the overpotential of the lithium plating reaction. When the current rate is large, the difference between the two will be obvious, as can be seen in the experimental results later in the article. The main innovation of this paper is that an equivalent circuit model for the half-cells is proposed so that the lithium plating reaction overpotential can be estimated, which truly reflects the onset point of plating. In addition, square wave current at a specific frequency is superimposed on the discharge current (equivalent to the charge process of full cells) so that impedance variation during discharging can be calculated in real time. Moreover, the IC curves of the subsequent charge process after discharge are also calculated as supplementary validation for lithium plating detection.

The remainder of the article is structured as follows: Section 2 outlines the methodology and experimental scheme. Section 3 comprises the detailed experimental conditions and procedures and shows the analysis and discussion of the experimental results. Section 4 concludes the whole article.

2. Materials and Methods

To obtain the potential changes in the graphite electrode (vs. Li/Li^+), the batteries used in the experiments are self-made half-cells: the positive electrode is graphite (areal active material loading is 6.3 mg/cm^2 and weight fraction is 93.2%), while the negative electrode is Li metal purchased from Hefei Kejing Material Technology Co., Hefei, China. The thickness of the graphite pole piece ranges from 40 to 60 μm. The separator adopts Celgard 2325, which was purchased from Shenzhen Kejing Star Technology Co., Shenzhen, China. The electrolyte is 1.0 M $LiPF_6$/EC+DEC (1:1), which was purchased from Duoduo Chem Co., Suzhou, China. Cell assembly was conducted in a glove box with Argon gas. The graphite electrodes were cut into 12 mm diameter disks and assembled into coin cells with Li metal counter electrodes. Several different half-cells were assembled with the same material and labeled, respectively.

The type of charge/discharge equipment used during the experiments was a NEWARE CT-4008Tn-5V10mA-HWX tester (NEWARE Technology Ltd., Shenzhen, China), the electrochemical impedance spectroscopy (EIS) test equipment was AMETEK PARSTAT 3000A-DX (AMETEK, Inc., Berwyn, PA, USA), and the model of the heating chamber was BINDER KB 53 (BINDER GmbH, Tuttlingen, Germany). The temperature of the experiments was set to 25 °C.

2.1. In Situ Impedance Test at Constant Frequency During Discharging

When the half-cell is discharging, lithium ions transfer from the negative electrode (Li metal) to the graphite electrode, which corresponds to the charging process of the full cell. During the discharge process, lithium ions may be deposited on the graphite electrode surface, i.e., lithium plating occurs. Two different types of experiments were carried out on the half-cells: one is overdischarging, which is equivalent to the overcharging of the full cells, and another is fast-discharging experiments. To obtain the impedance change during the discharge of the half-cell, a square wave current is injected into the discharge current. Fast Fourier transformation (FFT) is performed on the input square wave current and the battery terminal voltage to transform the time domain information into frequency domain information, so that the magnitude of the impedance at a specific frequency can be obtained. The detailed implemented method can be found in our previously published paper [37]. The half-cell is recharged after discharge to obtain the IC curve. The detection of the lithium plating of the half-cells during the discharge process is carried out by combing with the graphite anode potential and the IC curves. The diagram of the experimental procedure is shown in Figure 1.

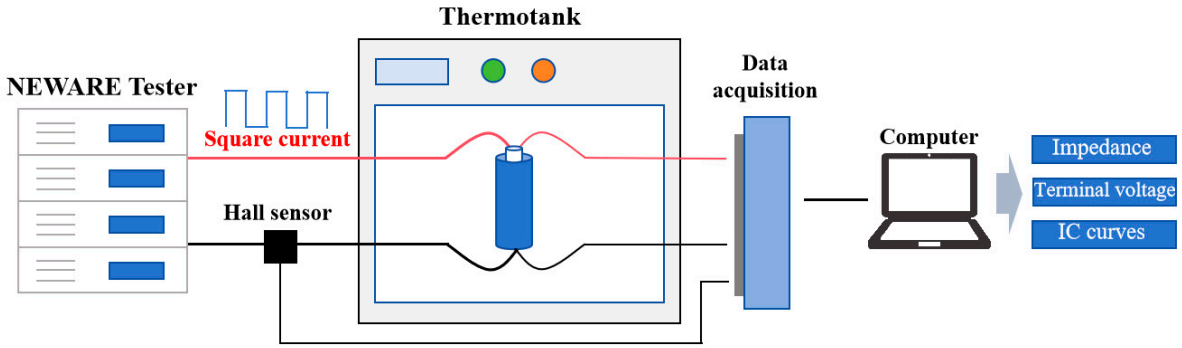

Figure 1. Schematic diagram of the experimental process.

2.2. Overpotential Estimation of Lithium Plating Based on Lithium–Graphite Half-Cells

Both the lithium plating and the normal lithium insertion occur on the graphite electrode, while the lithium plating occurs as a side reaction only when the reaction overpotential is below zero. As reported by Arora [39], the overpotential of the lithium plating follows the equation below [4]:

$$\eta_{Li}(z,t) = \phi_s(z,t) - \phi_e(z,t) - U_{Li} - i(z,t)R_{SEI}(z,t) \quad (1)$$

where ϕ_s is the solid phase potential; ϕ_e is the liquid phase potential; U_{Li} is the equilibrium potential for the lithium plating, which is considered 0 V; and iR_{SEI} is the potential loss resulting from the SEI. When η_{Li} reaches below 0 V, lithium plating becomes thermodynamically possible [40]. All physical quantities mentioned above are functions of spatial position z, which is shown in Figure 2.

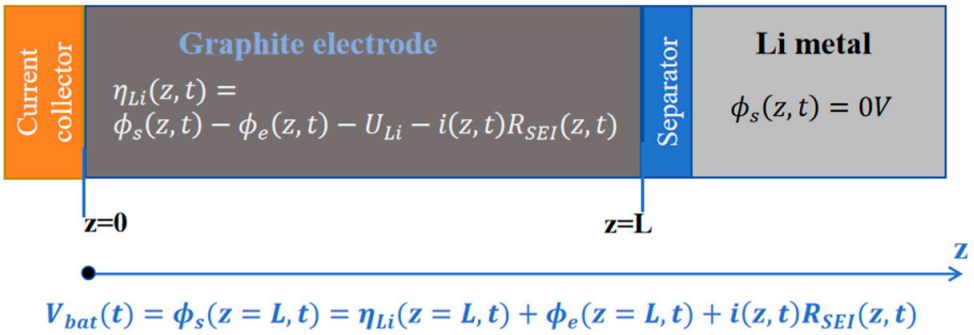

Figure 2. Schematic of graphite half-cell and local voltage relationships.

The local equilibrium potential E_{eq} is a function of the local intercalation fraction, which in turn is related to the lithium overpotential by

$$\eta_{Li}(z,t) = E_{eq}(z,t) + \eta_{Gr}(z,t) \quad (2)$$

where η_{Gr} is the graphite overpotential [41].

Taking the coordinates, as shown in Figure 2, since the lithium metal is at its reference voltage of 0 V, the cell voltage V_{bat} compared to the lithium metal electrode can be expressed as $V_{bat}(t) = \phi_s(z=0,t)$. Assuming the effective electronic conductivity of the graphite is much bigger than the ionic conductivity, the gradients of ϕ_s with respect to the position can be negligible. According to Aleksandar et al. [42], lithium plating first occurs near the separator, where the local intercalation fraction first reaches 100%. So, we can set the position at $z = L$.

$$V_{bat}(t) = \phi_s(z=L,t) = \eta_{Li}(z=L,t) + \phi_e(z=L,t) + i(z=L,t)R_{SEI}(z,t) \quad (3)$$

In Equation (3), V_{bat} is the terminal voltage of the battery and can be measured directly, but the physical indication of whether lithium plating occurs thermodynamically is the overpotential of the lithium plating reaction [4,5], and it cannot be directly measured. To estimate η_{Li}, a simplified equivalent circuit model considering lithium plating side reactions [43] is applied as depicted in Figure 3. The model reduces the graphite electrode to just one graphite particle, and the physical definitions of the variables in Figure 3 are given in Table 1. The superscripts "+" and "−" correspond to the positive and negative electrodes, respectively. The subscripts "*s*" and "*e*" correspond to solid phase and electrolyte phase.

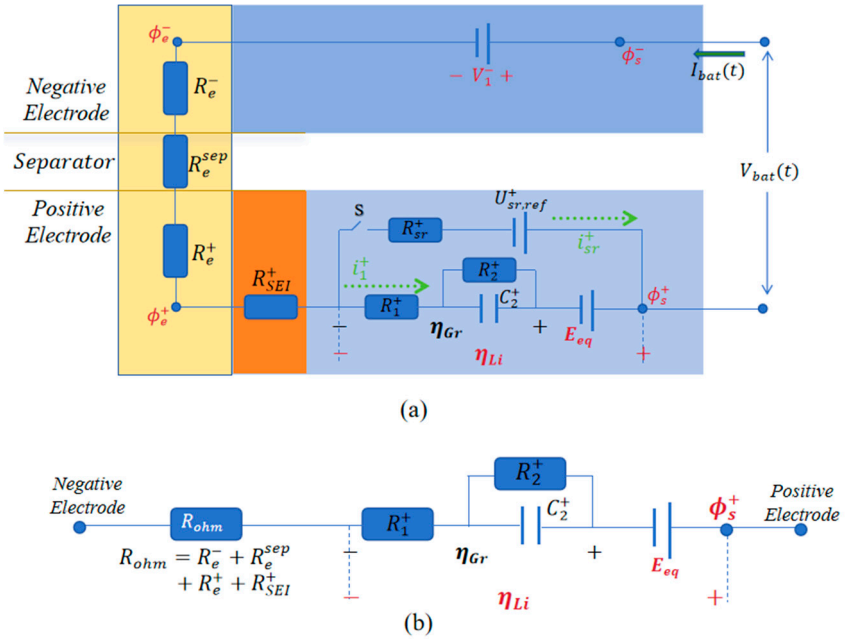

Figure 3. Equivalent circuit model considering lithium plating reactions. (**a**) ECM considering lithium plating. (**b**) Simplified ECM when lithium plating has not occurred.

Table 1. Physical definition of different voltage in the equivalent circuit model.

Symbols	Definition
V_1^-	Open circuit voltage of the Li metal electrode (vs. Li/Li$^+$), $V_1^- = 0$
E_{eq}	Equilibrium potential of graphite electrode vs. Li/Li$^+$
η_{Gr}	Graphite solid phase polarization potential
$U_{sr,ref}^+$	Equilibrium potential of lithium plating, $U_{sr,ref}^+ = 0$
R_{SEI}^+	Resistance of SEI membrane
$R_e^{\pm}$	Resistance of electrolyte
R_e^{sep}	Resistance of separator
$\phi_s^{\pm}$	Electrode solid phase potential
$\phi_e^{\pm}$	Electrode liquid phase potential
η_{Li}	Overpotential of lithium plating reaction
V_{bat}	Battery terminal voltage
I_{bat}	Battery charge/discharge current
i_1^+	Reaction current of normal lithium intercalation
i_{sr}^+	Reaction current of lithium plating reaction

Due to resistance existing in the electrolyte path and SEI, there is a slight deviation between the η_{Li} and terminal voltage of the half-cell [44]. When lithium plating has not yet occurred, i.e., the switch s in Figure 3 is not yet closed, this deviation is defined as V_{ohm}, which can be calculated as follows:

$$V_{ohm} = I_{bat} R_{ohm} = I_{bat}\left(R_{SEI}^+ + R_e^+ + R_e^{sep} + R_e^-\right) \quad (4)$$

The equivalent circuit model can be further simplified, as shown in Figure 3b. The simplified equivalent circuit model is regarded as total resistance R_{sum} followed by an RC in parallel, where $R_{sum} = R_{ohm} + R_1^+$. E_{eq} in Figure 3b is a function of the local intercalation fraction χ of the graphite particle. To calculate E_{eq}, here we assume that χ approximately equals to the battery SOC. Combined with the terminal voltage and the current I_{bat} during discharging, parameters R_{sum}, R_2^+, and C_2^+ can be identified in real time via the optimal estimation method. R_{ohm} and R_1^+ are in series, thus cannot be distinguished from each other. Assuming R_1^+ is much smaller than R_{ohm}, it can be approximated that $R_{sum} \approx R_{ohm}$. The real lithium plating overpotential η_{Li} is estimated and expressed as

$$\eta_{Li} \approx V_{bat} + I_{bat} R_{sum} \tag{5}$$

The obtained Equation (5) matches the conclusion or statements in reference articles [42,44]. It should be mentioned that in Equation (3), we pay attention to η_{Li} at position $z = L$, but to estimate this overpotential, we propose a simplified equivalent model in Figure 3 to describe the half-cell. So, the η_{Li} in Equation (5) is an averaged concept, and there are differences in between.

3. Experiments and Results

3.1. EIS Characterization of Half-Cells

To seek a constant frequency as the characteristic frequency applied in the following diagnosis of the lithium plating onset, the EIS of the self-made half-cells was measured at a constant temperature of 25 °C and at different SOCs, and the results are shown in Figure 4. As SOC changes, it can be observed that the impedance change within the moderate and low-frequency bands is most obvious, corresponding to the frequency range of approximately 1–100 Hz. Considering that the charge transfer process is highly related to SOC, it is reasonable to assume that the impedance change between 1 and 100 Hz mainly depends on the change in the charge transfer process [32,37,45]. The occurrence of lithium plating affects the charge transfer process inside the battery, so the frequency of the injected square-wave current during discharging is finally set to 1 Hz, i.e., the frequency of the fundamental wave obtained after fast Fourier transform of the discharge current and terminal voltage is 1 Hz. Furthermore, the impedance change at 1 Hz can also be calculated.

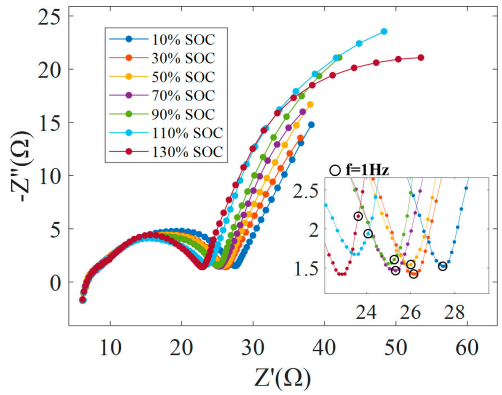

Figure 4. EISs of the half-cell at different SOCs.

3.2. Overdischarge Experiments

To investigate the relationship between impedance variation and lithium plating under the overdischarging of the half-cell (equivalent to overcharging of full cells), experiments were carried out on four different half-cells, labeled G1#1 to G1#4. Before the test, a cycle of constant current charge/discharge experiment is carried out, where the current is 0.2 mA and the voltage range is 0.01 V–2.0 V. Thus, the actual capacities of the four cells are identified as 2.0 mAh, 1.4 mAh, 2.2 mAh, and 1.7 mAh, respectively. The nominal capacity is taken as 2.0 mAh here.

In overdischarge experiments the discharge current is a square wave current with a period of 1 s, where 0.5 mA in 0.5 s and 0.3 mA in 0.5 s, so the average discharge current magnitude is 0.4 mA, i.e., about 0.2 C. The amplitude of the square-wave current is 0.2 mA and the amplitude of the battery terminal voltage response is roughly 10 mV, which is considered to be in the linear response region. The sampling period of current and of the terminal voltage is both 0.1 s. Based on current and voltage signals, the impedance at 1 Hz during the discharging process can be calculated by FFT, as well as the change in the real part. At the end of the discharge process, the cells are directly recharged at a constant current of 0.2 mA, and the IC curve can be obtained from the charging data to help evaluate whether lithium plating occurs.

For comparison validation, four cells are overdischarged at different depths, G1#1, G1#2, G1#3, and G1#4, corresponding to 105%, 110%, 120%, and 156% depth of discharge (DOD), respectively. Lithium ions move towards the graphite electrode in this process, and the x-axis of Figure 5 indicates the lithiation degree of the graphite electrode. Since the discharge current is still small, the difference between the battery terminal voltage and the overpotential η_{Li} is also tiny. Therefore, in this section these two physical quantities are not distinguished in detail.

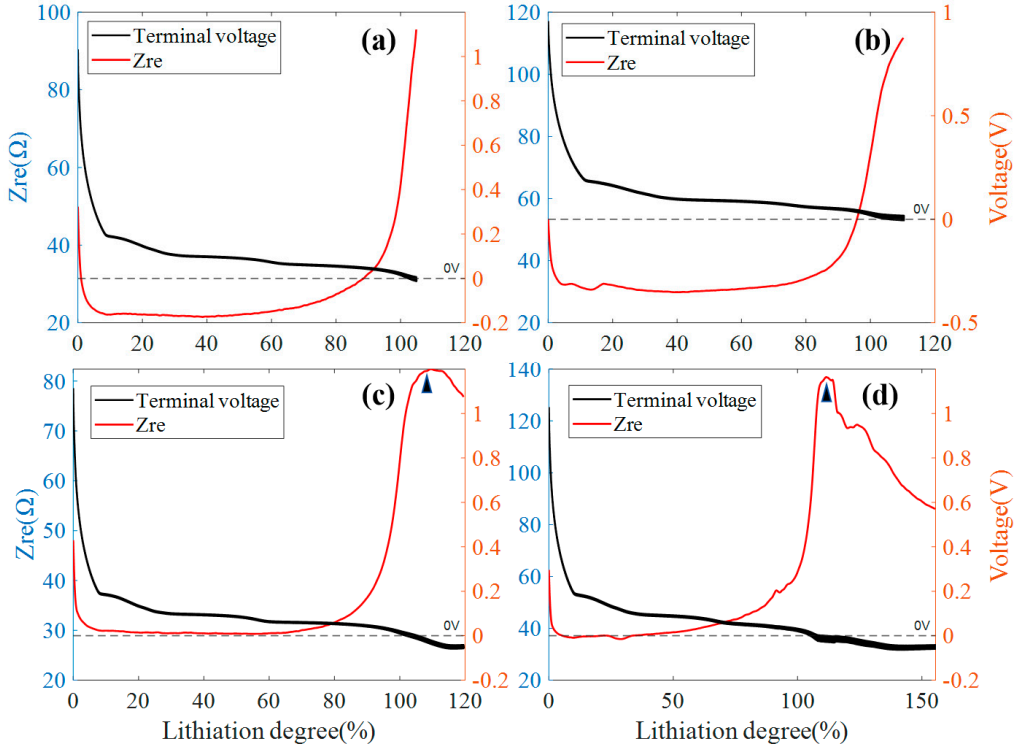

Figure 5. The evolution of the real part of 1 Hz impedance and terminal voltage during over discharging. (**a**) G1#1, (**b**) G1#2, (**c**) G1#3, (**d**) G1#4.

Figure 5 shows the variation in the terminal voltage and the real part of the 1 Hz impedance of four half-cells. In Figure 5a,b, for G1#1 and G1#2 with minor discharge depths, we can see that the terminal voltage of these two cells remains above 0 V and the real part of their impedance at 1 Hz frequency keeps increasing in the late stage, except for a decreasing trend in the early stage. In Figure 5c,d, for cells G1#3 and G1#4 with discharge depths of 120% and 156%, the terminal voltage decreases to below 0 V in the late stage of discharge, and the real part of the 1 Hz impedance has a turning point at a later stage, marked by "▲" in Figure 5c,d, after which the magnitude gradually decreases. The exact lithiation degrees, corresponding to the zero point of terminal voltage and the inflection point of the impedance, are listed in Table 2. The zero point and the inflection point correspond to nearly the same graphite lithiation degree, i.e., also the same time point.

Table 2. Lithiation degree, corresponding to the inflection points of the impedance and the zero points of the overpotential.

	Overdischarge 120%	Overdischarge 156%	Fast Discharge 0.75 C	Fast Discharge 1 C	Fast Discharge 1.5 C	Fast Discharge 3 C
Impedance inflection	108%	110%	95%	75%	63%	47%
Overpotential zero point	106%	110%	85%	65%	50%	31%

As auxiliary verification, the terminal voltage variation and IC curves during the subsequent charging process of the four half-cells were researched, as shown in Figures 6 and 7, where the charging voltage plateaus ①②③④ in Figure 6a–d correspond to the peaks A, B, C, and D in Figure 7a–d, respectively. Combined with Figure 5, for cells G1#1 and G1#2 with 105% DOD and 110% DOD, their terminal voltages were always above 0 V during the discharging, and the real part of the impedance remained increasing during the late stage. There is also no abnormal lithium plating peak in the IC curves in Figure 7a,b, indicating that no lithium plating occurred during discharging. Otherwise, for G1#3 and G1#4 cells with DODs of 120% and 156%, the terminal voltage gradually drops below 0 V, and the real part of the impedance shows a turning point in Figure 5. Correspondingly, there is also an abnormal lithium plating peak (peak A) in the IC curves, which is marked with "▲" in Figure 7c,d, indicating that lithium plating occurred during the discharging process.

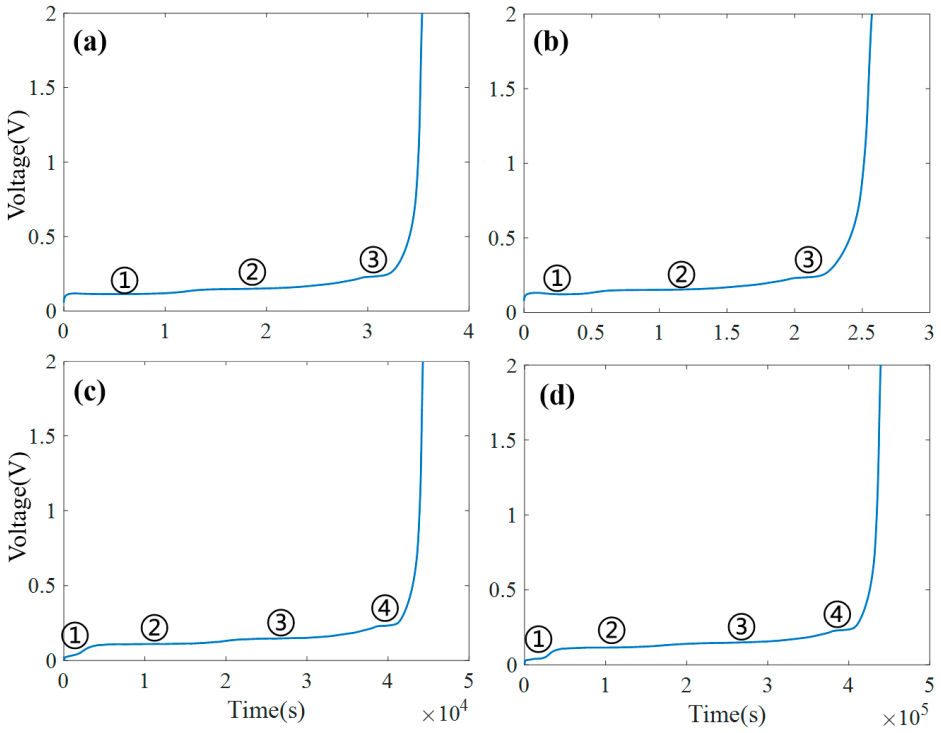

Figure 6. Variation in terminal voltage during the charging processes of four half-cells. (**a**) G1#1, (**b**) G1#2, (**c**) G1#3, (**d**) G1#4.

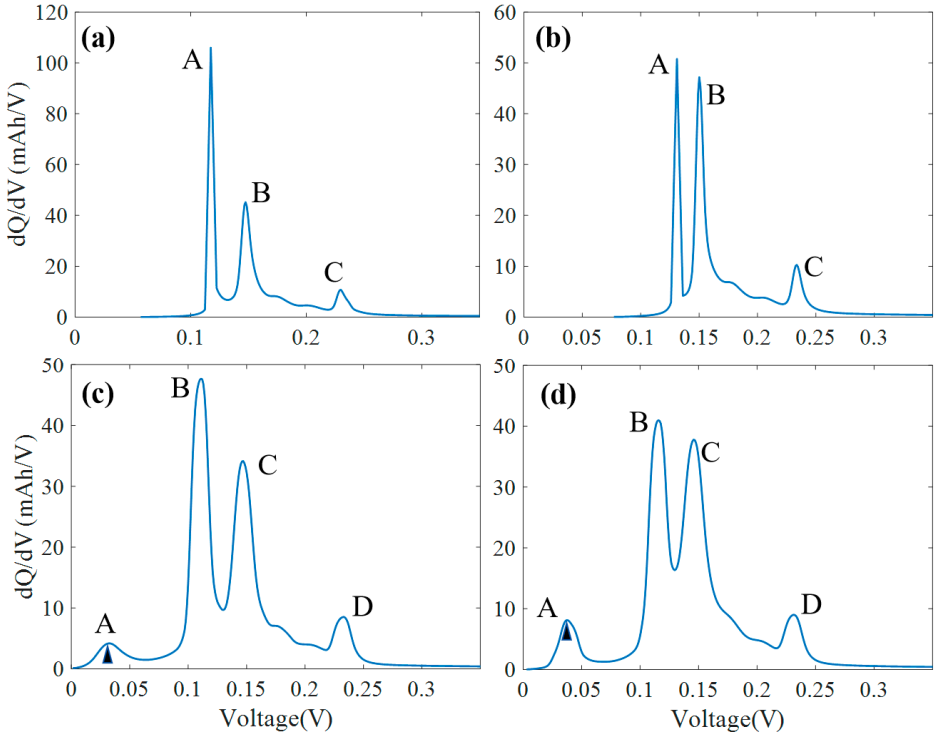

Figure 7. IC curves during charging of four half-cells. (**a**) G1#1, (**b**) G1#2, (**c**) G1#3, (**d**) G1#4.

The explanation for the appearance of the impedance inflection point is the introduction of the parallel resistance R_{sr}^{+} when lithium plating occurs, as shown in Figure 3. This introduced parallel resistance will reduce the overall impedance. Similar discussions can also be found in the reference [36,37,46]. In total, the above experimental results show that there is a direct relationship between lithium plating, graphite potential falling below 0 V, and the turning point of the impedance variation curve. Since the discharge current is very small, battery terminal voltage and lithium plating overpotential are not distinguished in detail in this section. According to the experimental results, when the potential of graphite electrode (vs. Li/Li^{+}) drops below 0 V, lithium plating becomes thermodynamically possible [44], and the real part of 1 Hz impedance tends to decrease after lithium plating occurs.

3.3. Fast Discharge Experiments

To explore the relationship between the onset of lithium plating and the abnormal trend in impedance under the fast-charging scenario for a full cell, fast-discharging experiments were carried out on another half-cell labeled as G2#1. Before the fast discharge experiments started, the cell was subjected to a constant current charge and discharge experiment at the magnitude of 0.2 mA, and its actual capacity was measured to be 2.2 mAh.

For fast discharge of G2#1, four different discharge rates were adopted: 0.75 C, 1 C, 1.5 C, and 3 C. Four experiments were performed sequentially. The cell was first discharged at 0.75 C rate to a discharge depth of 100%, and immediately after that it was charged at a constant current of 0.1 C to 2.0 V to obtain the IC curve during the charging process. The cell was then left to stand for 1 h after the end of charging. Afterwards, the fast discharge experiment was conducted at 1C rate, which was identical to the previous experiment except for the difference in discharge rate. This procedure was repeated until at last the fast discharge experiment at 3 C and the charge process at rate 0.1 C were performed. In all four experiments, the discharge current was a square wave with a period of 1s and a DC bias of 0.75 C, 1 C, 1.5 C, and 3 C, respectively. The amplitude of the square-wave current was set to 0.2 mA, which is the same as in the overdischarge experiments.

Figure 8 shows the impedance variation, measured terminal voltage, and estimated lithium plating overpotential during the discharge process. As shown in Figure 8a–d, when

the discharge current increases, the difference between cell terminal voltage and lithium plating overpotential becomes more and more pronounced. Based on Equations (3)–(5), the lithium plating overpotential can be estimated using the optimal estimation method, which is indicated by the blue lines in Figure 8a–d and was used to assist in determining whether and when lithium plating occurs.

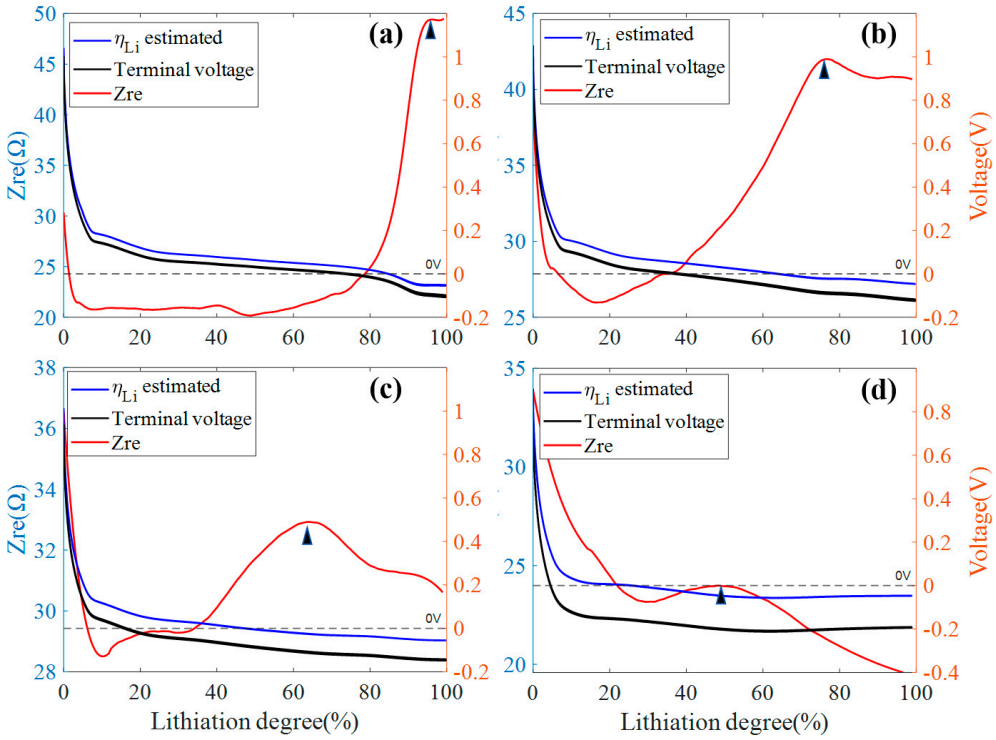

Figure 8. Real part of 1 Hz impedance, terminal voltage, and estimated overpotential in discharge process. (**a**) Discharge rate 0.75 C, (**b**) discharge rate 1 C, (**c**) discharge rate 1.5 C, and (**d**) discharge rate 3 C.

Figure 9 shows the IC curves during the subsequent charge process, which is taken as the auxiliary verification of lithium plating. In Figure 8a, with a current of 0.75 C, the cell terminal voltage and estimated lithium plating overpotential stayed above 0 V in the early stages, and the impedance stayed on an upward trend in the middle and late stages. When the graphite lithiation degree reaches about 90%, the lithium plating overpotential drops to slightly below 0 V, and the real part of the impedance also shows an inflection point, but it does not decrease too much. These two phenomena imply a small amount of lithium plating. In Figure 9b, from the IC curves we can also see there is only a very small peak for 0.75 C discharge experiments, which also indicate there is only a tiny amount of lithium plating during discharging.

In Figure 8b,d, we can see that the cell terminal voltage quickly dropped below 0 V. For example, in the 1.5 C discharge experiment, the cell terminal voltage dropped below 0 V at only 18% graphite lithiation degree. It is inaccurate to use the terminal voltage of the half-cell to predict whether or when lithium plating has occurred. However, there is a better and stronger correspondence between the estimated lithium plating overpotential and the impedance change trends. In Figure 8b,d, the impedance shows a decreasing trend at the very beginning, starts to increase afterwards, and shows a decreasing inflection point afterwards in the middle or late stages. The appearance of the inflection point indicates the occurrence of lithium plating: on the one hand, the moment corresponding to the inflection point is nearly the same as the zero point of the estimated η_{Li}; and on the other hand, the characteristic peak of lithium plating in the IC curves, which is marked with "▲" in Figure 9b, also proves that lithium plating did occur.

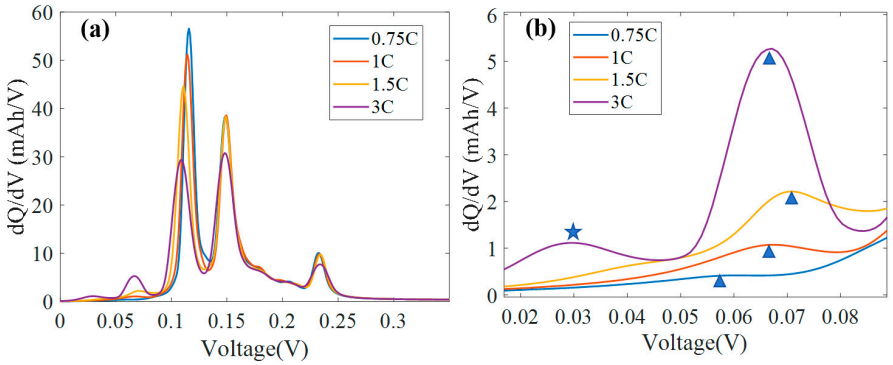

Figure 9. IC curves during the charge process in the fast discharge experiments. (**a**) IC curves; (**b**) partial enlargement.

The exact lithiation degree of the impedance inflection point and the overpotential zero point are also listed in Table 2. It is worth noting that the zero point of the estimated overpotential could be slightly earlier than the inflection point of the impedance, as shown in Table 2. And as the current rate increases, the difference between the two also tends to become larger. This could be explained in two ways: (1) In Section 2.2, E_{eq} should ideally be a function of the local intercalation fraction of the graphite particle, but to estimate the average lithium plating overpotential of the graphite electrode, E_{eq} is estimated as a function of the battery SOC, which leads to errors. For the position at the point near the separator, the local intercalation fraction is actually higher than the battery SOC. So, the calculated E_{eq} is higher than the actual value, which leads to a higher estimated R_{sum} and also a higher estimated η_{Li}, i.e., the actual overpotential near the separator will be lower. Reversely, for the position near the current collector, the actual overpotential will be higher. When the current rate goes up, the gradient of overpotential inside the whole graphite electrode will also become larger. (2) When only a trace amount of lithium is plated, the impedance will probably not drop immediately but will continue to maintain the previous upward trend, i.e., the inflection point of the impedance will occur only when the amount of the plated lithium reaches a certain level.

It is also worth mentioning that in the IC curves in Figure 9b for the 3 C rate experiments, in addition to the characteristic peak of lithium plating, there is another peak in a smaller voltage interval, which is marked by "★" in Figure 9b. This may be due to the occurrence of other side reactions other than lithium plating.

To conclude, in all four fast discharging tests at different current rates, the abnormal inflection point of impedance at 1 Hz coincides closely with the time point where the estimated overpotential of the lithium plating reaction reaches zero. Combining with the analysis of IC curves, it is further proven that the abnormal inflection point of impedance can be basically regarded as the onset of lithium plating.

4. Conclusions

In this study, by measuring the potential of the graphite electrode (vs. Li/Li^+) in the half-cells and combining with the IC curves, the direct relationship between the onset of lithium plating and abnormal impedance changes is confirmed through the overdischarging and fast-discharging experiments of lithium–graphite half-cells. To estimate the real overpotential of the lithium plating reaction, an equivalent circuit model for the half-cell is proposed and applied. When no lithium plating occurs, the 1 Hz impedance of the half-cell during discharging shows a rising trend in the middle-late stages, and the lithium plating reaction overpotential η_{Li} maintains above 0 V. Lithium plating drops the overpotential η_{Li} below 0 V, and the impedance will also show an inflection point and then start to decrease in the middle and late stages. In both overdischarge and fast-discharge experiments, the abnormal inflection point of the impedance and the zero point of the estimated lithium plating overpotential occur nearly. This proves that the abnormal inflection point of impedance can

be basically regarded as the onset of lithium plating. Cross-validation between impedance variation trends, IC curves, and estimated lithium plating overpotentials corroborate the validity of using abnormal impedance trends to determine the onset of lithium plating.

Our future work will focus on the following: (1) developing a half-cell P2D model containing lithium plating side reactions and calculating the localized graphite particle intercalation fraction and localized lithium plating overpotential to further validate the conclusions, and (2) studying the effects of temperature on the conclusions obtained above.

Author Contributions: Conceptualization: Z.J.; data curation: J.W.; writing—original draft: J.W. and W.W.; visualization: H.L.; software: B.L.; conceptualization: X.W. (Xueyuan Wang); writing—review and editing: J.J., H.D. and X.W. (Xuezhe Wei). All authors have read and agreed to the published version of the manuscript.

Funding: This work was financially supported by the National Natural Science Foundation of China (grant number: 52207242, U20A20310), the Project of Ningbo Automotive Electronics Intelligentification Innovation Union (2022H007), Project of Zhejiang LingYan Plan (2024C01249(SD2)), and Project of Ningbo Sicence and Technology of Yongjiang 2035 (2024Z068).

Data Availability Statement: The data of this study are available from the corresponding authors upon request.

Conflicts of Interest: Author Zhao Jiang was employed by the company Ningbo Joyson Advanced Energy Research Institute Co., Ltd. Author Bingyin Luo was employed by the company ICBG China Resources Microelectronics Co., Ltd. The remaining authors declare that the research was conducted in the absence of any commercial or financial relationships that could be construed as a potential conflict of interest.

References

1. Cai, W.L.; Yao, Y.X.; Zhu, G.L.; Yan, C.; Jiang, L.L.; He, C.X.; Huang, J.Q.; Zhang, Q. A review on energy chemistry of fast-charging anodes. *Chem. Soc. Rev.* **2020**, *49*, 3806–3833. [CrossRef] [PubMed]
2. Ahmed, S.; Bloom, I.; Jansen, A.N.; Tanim, T.; Dufek, E.J.; Pesaran, A.; Burnham, A.; Carlson, R.B.; Dias, F.; Hardy, K.; et al. Enabling fast charging—A battery technology gap assessment. *J. Power Sources* **2017**, *367*, 250–262. [CrossRef]
3. Ouyang, M.G.; Ren, D.S.; Lu, L.G.; Li, J.Q.; Feng, X.N.; Han, X.B.; Liu, G.M. Overcharge-induced capacity fading analysis for large format lithium-ion batteries with $Li_yNi_{1/3}Co_{1/3}Mn_{1/3}O_2$ + $LiyMn_2O_4$ composite cathode. *J. Power Sources* **2015**, *279*, 626–635. [CrossRef]
4. Ren, D.S.; Smith, K.; Guo, D.X.; Han, X.B.; Feng, X.N.; Lu, L.G.; Ouyang, M.G.; Li, J.Q. Investigation of Lithium Plating-Stripping Process in Li-Ion Batteries at Low Temperature Using an Electrochemical Model. *J. Electrochem. Soc.* **2018**, *165*, A2167–A2178. [CrossRef]
5. Legrand, N.; Knosp, B.; Desprez, P.; Lapicque, F.; Raël, S. Physical characterization of the charging process of a Li-ion battery and prediction of Li plating by electrochemical modelling. *J. Power Sources* **2014**, *245*, 208–216. [CrossRef]
6. Waldmann, T.; Hogg, B.I.; Wohlfahrt-Mehrens, M. Li plating as unwanted side reaction in commercial Li-ion cells—A review. *J. Power Sources* **2018**, *384*, 107–124. [CrossRef]
7. Li, Z.; Huang, J.; Liaw, B.Y.; Metzler, V.; Zhang, J.B. A review of lithium deposition in lithium-ion and lithium metal secondary batteries. *J. Power Sources* **2014**, *254*, 168–182. [CrossRef]
8. Ouyang, M.G.; Chu, Z.Y.; Lu, L.G.; Li, J.Q.; Han, X.B.; Feng, X.N.; Liu, G.M. Low temperature aging mechanism identification and lithium deposition in a large format lithium iron phosphate battery for different charge profiles. *J. Power Sources* **2015**, *286*, 309–320. [CrossRef]
9. Feng, X.; He, X.; Lu, L.; Ouyang, M. Analysis on the Fault Features for Internal Short Circuit Detection Using an Electrochemical-Thermal Coupled Model. *J. Electrochem. Soc.* **2018**, *165*, A155–A167. [CrossRef]
10. Feng, X.N.; Zhang, F.S.; Huang, W.S.; Peng, Y.; Xu, C.S.; Ouyang, M.G. Mechanism of internal thermal runaway propagation in blade batteries. *J. Energy Chem.* **2024**, *89*, 184–194. [CrossRef]
11. Brissot, C.; Rosso, M.; Chazalviel, J.N.; Baudry, P.; Lascaud, S. In situ study of dendritic growth in lithium/PEO-salt/lithium cells. *Electrochim. Acta* **1998**, *43*, 1569–1574. [CrossRef]
12. Ringbeck, F.; Rahe, C.; Fuchs, G.; Sauer, D.U. Identification of Lithium Plating in Lithium-Ion Batteries by Electrical and Optical Methods. *J. Electrochem. Soc.* **2020**, *167*, 090536. [CrossRef]
13. Honbo, H.; Takei, K.; Ishii, Y.; Nishida, T. Electrochemical properties and Li deposition morphologies of surface modified graphite after grinding. *J. Power Sources* **2009**, *189*, 337–343. [CrossRef]
14. Arai, J.; Nakahigashi, R. Study of Li Metal Deposition in Lithium Ion Battery during Low-Temperature Cycle Using In Situ Solid-State Li Nuclear Magnetic Resonance. *J. Electrochem. Soc.* **2017**, *164*, A3403–A3409. [CrossRef]

15. de Araujo, L.A.; Sarou-Kanian, V.; Sicsic, D.; Deschamps, M.; Salager, E. Operando nuclear magnetic resonance spectroscopy: Detection of the onset of metallic lithium deposition on graphite at low temperature and fast charge in a full Li-ion battery. *J. Magn. Reson.* **2023**, *354*, 107527. [CrossRef]
16. Arora, P.; Doyle, M.; White, R.E. Mathematical modeling of the lithium deposition overcharge reaction in lithium-ion batteries using carbon-based negative electrodes. *J. Electrochem. Soc.* **1999**, *146*, 3543–3553. [CrossRef]
17. Adam, A.; Knobbe, E.; Wandt, J.; Kwade, A. Application of the differential charging voltage analysis to determine the onset of lithium-plating during fast charging of lithium-ion cells. *J. Power Sources* **2021**, *495*, 229794. [CrossRef]
18. Mei, W.X.; Jiang, L.H.; Liang, C.; Sun, J.H.; Wang, Q.S. Understanding of Li-plating on graphite electrode: Detection, quantification and mechanism revelation. *Energy Storage Mater.* **2021**, *41*, 209–221. [CrossRef]
19. Chen, Y.X.; Torres-Castro, L.; Chen, K.H.; Penley, D.; Lamb, J.; Karulkar, M.; Dasgupta, N.P. detection of Li plating during fast charging of Li-ion batteries using incremental capacity analysis. *J. Power Sources* **2022**, *539*, 231601. [CrossRef]
20. Schmidt, J.P.; Adam, A.; Wandt, J. Time-Resolved and Robust Lithium Plating Detection for Automotive Lithium-Ion Cells with the Potential for Vehicle Application. *Batteries* **2023**, *9*, 97. [CrossRef]
21. Strasser, A.; Adam, A.; Li, J.H. In operando detection of Lithium plating via electrochemical impedance spectroscopy for automotive batteries. *J. Power Sources* **2023**, *580*, 233366. [CrossRef]
22. Wang, H.; Song, Y.J.; Sun, X.; Mo, S.K.; Chen, C.; Wang, J.J. Onboard in-situ warning and detection of Li plating for fast-charging batteries with deep learning. *Energy Storage Mater.* **2024**, *71*, 103585. [CrossRef]
23. Doyle, M.; Fuller, T.F.; Newman, J. Modeling of Galvanostatic Charge and Discharge of the Lithium/Polymer/Insertion Cell (vol 140, pg 1526, 1993). *J. Electrochem. Soc.* **2018**, *165*, X13. [CrossRef]
24. Lu, Y.F.; Han, X.B.; Chu, Z.Y.; Feng, X.N.; Qin, Y.D.; Ouyang, M.G.; Lu, L.G. A decomposed electrode model for real-time anode potential observation of lithium-ion batteries. *J. Power Sources* **2021**, *513*, 230529. [CrossRef]
25. Zhao, T.Z.; Zheng, Y.J.; Liu, J.H.; Zhou, X.; Chu, Z.Y.; Han, X.B. A study on half-cell equivalent circuit model of lithium-ion battery based on reference electrode. *Int. J. Energy Res.* **2021**, *45*, 4155–4169. [CrossRef]
26. von Lüders, C.; Zinth, V.; Erhard, S.V.; Osswald, P.J.; Hofmann, M.; Gilles, R.; Jossen, A. Lithium plating in lithium-ion batteries investigated by voltage relaxation and in situ neutron diffraction. *J. Power Sources* **2017**, *342*, 17–23. [CrossRef]
27. Schindler, S.; Bauer, M.; Petzl, M.; Danzer, M.A. Voltage relaxation and impedance spectroscopy as in-operando methods for the detection of lithium plating on graphitic anodes in commercial lithium-ion cells. *J. Power Sources* **2016**, *304*, 170–180. [CrossRef]
28. Petzl, M.; Danzer, M.A. Nondestructive detection, characterization, and quantification of lithium plating in commercial lithium-ion batteries. *J. Power Sources* **2014**, *254*, 80–87. [CrossRef]
29. Smart, M.C.; Ratnakumar, B.V. Effects of Electrolyte Composition on Lithium Plating in Lithium-Ion Cells. *J. Electrochem. Soc.* **2011**, *158*, A379–A389. [CrossRef]
30. Chen, Y.J.; Zhang, H.Q.; Hong, J.C.; Hou, Y.K.; Yang, J.S.; Zhang, C.; Ma, S.K.; Zhang, X.Y.; Yang, H.X.; Liang, F.W.; et al. Lithium plating detection of lithium-ion batteries based on the improved variance entropy algorithm. *Energy* **2024**, *299*, 131574. [CrossRef]
31. Harting, N.; Wolff, N.; Krewer, U. Identification of Lithium Plating in Lithium-Ion Batteries using Nonlinear Frequency Response Analysis (NFRA). *Electrochim. Acta* **2018**, *281*, 378–385. [CrossRef]
32. Chen, X.; Li, L.Y.; Liu, M.M.; Huang, T.; Yu, A.S. Detection of lithium plating in lithium-ion batteries by distribution of relaxation times. *J. Power Sources* **2021**, *496*, 229867. [CrossRef]
33. Brown, D.E.; McShane, E.J.; Konz, Z.M.; Knudsen, K.B.; McCloskey, B.D. Detecting onset of lithium plating during fast charging of Li-ion batteries using operando electrochemical impedance spectroscopy. *Cell Rep. Phys. Sci.* **2021**, *2*, 100589. [CrossRef]
34. Wang, Y.; Zhou, X.; Wang, R.X.; Zhang, T.; Xiao, P.T.; Si, Y.P.; Xiao, Y.K.; Liu, Y.J. High sensitivity detection of lithium plating in high-energy lithium-ion batteries based on time-domain distribution relaxation times analysis. *Energy Storage Mater.* **2024**, *69*, 103369. [CrossRef]
35. Sun, T.; Li, Z.; Zhu, G.Y.; Wang, L.Y.; Ren, D.S.; Shen, T.T.; Lu, L.G.; Zheng, Y.J.; Han, X.B.; Ouyang, M.G. Impedance-based online detection of lithium plating for lithium-ion batteries: Mechanism and sensitivity analysis. *Electrochim. Acta* **2024**, *496*, 144512. [CrossRef]
36. Koseoglou, M.; Tsioumas, E.; Ferentinou, D.; Jabbour, N.; Papagiannis, D.; Mademlis, C. Lithium plating detection using dynamic electrochemical impedance spectroscopy in lithium-ion batteries. *J. Power Sources* **2021**, *512*, 230508. [CrossRef]
37. Wang, X.Y.; Li, J.W.; Chen, S.Q.; Zhang, G.X.; Jiang, B.; Wei, X.Z.; Dai, H.F. Online Detection of Lithium Plating Onset for Lithium-Ion Batteries Based on Impedance Changing Trend Identification During Charging Processes. *IEEE Trans. Transp. Electrif.* **2023**, *9*, 3487–3497. [CrossRef]
38. Shen, Y.D.; Wang, X.Y.; Jiang, Z.; Luo, B.Y.; Chen, D.D.; Wei, X.Z.; Dai, H.F. Online detection of lithium plating onset during constant and multistage constant current fast charging for lithium-ion batteries. *Appl. Energy* **2024**, *370*, 123631. [CrossRef]
39. Arora, P.; White, R.E.; Doyle, M. Capacity fade mechanisms and side reactions in lithium-ion batteries. *J. Electrochem. Soc.* **1998**, *145*, 3647–3667. [CrossRef]
40. Randall, A.V.; Perkins, R.D.; Zhang, X.C.; Plett, G.L. Controls oriented reduced order modeling of solid-electrolyte interphase layer growth. *J. Power Sources* **2012**, *209*, 282–288. [CrossRef]
41. Gao, T.; Han, Y.; Fraggedakis, D.; Das, S.; Zhou, T.T.; Yeh, C.N.; Xu, S.M.; Chueh, W.C.; Li, J.; Bazant, M.Z. Interplay of Lithium Intercalation and Plating on a Single Graphite Particle. *Joule* **2021**, *5*, 393–414. [CrossRef]

42. Mijailovic, A.S.; Wang, G.Y.; Luo, M.; Lu, W.Q.; Wu, Q.L.; Sheldon, B.W. A "Master Curve" Describing Reaction Inhomogeneity and Plating Onset during Fast-Charging of Graphite Electrodes. *J. Electrochem. Soc.* **2023**, *170*, 070508. [CrossRef]
43. Li, Y.; Vilathgamuwa, M.; Choi, S.S.; Farrell, T.W.; Tran, N.T.; Teague, J. Development of a degradation-conscious physics-based lithium-ion battery model for use in power system planning studies. *Appl. Energy* **2019**, *248*, 512–525. [CrossRef]
44. Rodrigues, M.T.F.; Kalaga, K.; Trask, S.E.; Dees, D.W.; Shkrob, I.A.; Abraham, D.P. Fast Charging of Li-Ion Cells: Part I. Using Li/Cu Reference Electrodes to Probe Individual Electrode Potentials. *J. Electrochem. Soc.* **2019**, *166*, A996–A1003. [CrossRef]
45. Yi, M.; Jiang, F.; Zhao, G.; Guo, D.; Ren, D.; Lu, L.; Ouyang, M. Detection of lithium plating based on the distribution of relaxation times. In Proceedings of the 2021 IEEE 4th International Electrical and Energy Conference (CIEEC), Wuhan, China, 28–30 May 2021; pp. 1–5.
46. Katzer, F.; Rüther, T.; Plank, C.; Roth, F.; Danzer, M.A. Analyses of polarisation effects and operando detection of lithium deposition in experimental half- and commercial full-cells. *Electrochim. Acta* **2022**, *436*, 141401. [CrossRef]

Disclaimer/Publisher's Note: The statements, opinions and data contained in all publications are solely those of the individual author(s) and contributor(s) and not of MDPI and/or the editor(s). MDPI and/or the editor(s) disclaim responsibility for any injury to people or property resulting from any ideas, methods, instructions or products referred to in the content.